Electric Double Layer at the Rutile (110) Surface. 1. Structure of Surfaces and Interfacial Water from Molecular Dynamics by Use of ab Initio Potentials

M. Předota,*,†,‡ **A. V. Bandura,**§,‖ **P. T. Cummings,**‡,⊥ **J. D. Kubicki,**§ **D. J. Wesolowski,**⊥ **A. A. Chialvo,**⊥ **and M. L. Machesky**▽

Institute of Chemical Process Fundamentals, Academy of Sciences of the Czech Republic, 165 02 Prague, Czech Republic, Department of Chemical Engineering, Vanderbilt University, Nashville, Tennessee 37235-1604, Department of Health Physics and Biophysics, Faculty of Health and Social Studies, University of South Bohemia, Jírovcova 24, České Budějovice 370 04, Czech Republic, Department of Geosciences, The Pennsylvania State University, University Park, Pennsylvania 16802, St. Petersburg State University, St. Petersburg, Russia, Chemical Sciences Division, Oak Ridge National Laboratory, Oak Ridge, Tennessee 37831-6110, and Illinois State Water Survey, Champaign, Illinois 61820

A recently developed force field for interactions of water molecules with the (110) surface of rutile (α-TiO$_2$) has been generalized for atomistically detailed molecular dynamics simulations of the interfacial structure of the uncharged mineral surface in contact with liquid SPC/E water at 298 K and 1 atm and for negatively charged surfaces in contact with SPC/E water containing dissolved electrolyte ions (Rb$^+$, Sr^{2+}, Zn^{2+}, Na$^+$, Ca^{2+}, Cl$^-$). Both hydroxylated (dissociative) and nonhydroxylated (associative) surfaces are simulated, since both types of water–surface interactions have been postulated from ab initio calculations and spectroscopic studies under near-vacuum conditions. The positions of water molecules at the interface were found to be very similar for both hydroxylated and nonhydroxylated surfaces, with either terminal hydroxyl groups or associated water molecules occupying the site above each terminal titanium atom. Beyond these surface oxygens, a single additional layer of adsorbed water molecules occupies distinct sites related to the underlying crystal surface structure. The water structure and mobility quickly decay to the bulk liquid properties beyond this second layer. The hydrogen-bonding structure and water orientation in these first two oxygen layers are somewhat sensitive to the hydroxylation of the surface, as are the electrostatic profiles. For all simulated properties, including space-dependent diffusivity of water molecules, the influence of the interface is negligible beyond distances of about 15 Å from the surface. Increasing the temperature to 448 K while maintaining the density at the liquid–vapor saturated condition had minimal effect on the interfacial structure and electrostatic properties. These results are foundational to the simulation of dissolved ion interactions with the surface and the comparison of the simulation results with X-ray standing wave and crystal truncation rod measurements of water and electrolyte solutions in contact with rutile (110) single-crystal surfaces presented in Part 2 of this series.

1. Introduction

Mineral−aqueous electrolyte solution interfaces are of common occurrence in natural and industrial environments. In the interfacial region, the solution properties and the crystal structure both deviate from the characteristics of the bulk phases.[1] The surface adsorption of ionic species from the aqueous solution generates an accumulation of net charge at the surface that must be balanced by countercharges in the fluid vicinity of the interface and the chemical interaction of water with the mineral surface involves water dissociation and a variety of acid−base reactions involving successive surface protonation states.[2,3] This interfacial region, termed the electrical double layer (EDL), exerts a profound influence on the stability and transport properties of colloids, the mobilities of trace elements in aqueous

solutions in contact with solid phases, nutrient bioavailability and bacterial attachment, corrosion, crystal nucleation and growth, and a myriad of natural and industrial processes.

The description of the surface charging process on metal oxides has been made traditionally through one-site/two-pK models, i.e., by assuming that the protonation (deprotonation) process characterizing the amphoteric nature of the surface takes place on a single (chemically homogeneous) type of surface site.[4] Typically these fluid−surface interactions are assessed by titration and electrokinetic measurements, methods that provide valuable information about the average physicochemical affinities of the mineral surfaces present, regardless of the true nature of specific interaction sites. Recently, the revised multisite complexation (MUSIC) model has been developed,[5−7] which quantitatively predicts the partial charges and proton affinities of the various types of surface oxygen sites, as aided by the structural analysis of mineral surfaces[8] and application of bond-valence principles. The MUSIC model is based on the idea of local charge cancellation;[9] that is, the charge on an atomic site on the surface can be treated as if distributed over all ligands surrounding the site, with each site bearing a partial charge

---

* Corresponding author: e-mail predota@icpf.cas.cz.
† Academy of Sciences of the Czech Republic and University of South Bohemia.
‡ Vanderbilt University.
§ The Pennsylvania State University.
‖ St. Petersburg State University.
⊥ Oak Ridge National Laboratory.
▽ Illinois State Water Survey.

inversely proportional to the site's coordination number. In addition to surface protonation, full charge compensation requires a plausible description of the structure of the electric double layer, usually accounted for by some form of the Stern model of specific ion binding at a discrete plane or planes, coupled with a Gouy−Chapman description of the diffuse layer of ion concentrations decaying out to the bulk solution composition.[10] Combined thermodynamic models of surface protonation, counterion affinities, and double layer structure are collectively termed surface complexation models (SCMs). However, fitting macroscopic surface titration and ion adsorption data to SCMs is ambiguous since the resulting ion binding constants and Stern-layer capacitance values can take on a range of plausible values.[11,12] Molecular simulation can provide detailed descriptions of electrical double layer structure, consistent with the microscopic fluid environment and the structure of the exposed surface, and thereby help remove the arbitrariness associated with the application of SCMs. Furthermore, such simulations can directly connect with various experimental determinations of the near surface structure and bonding properties.

In principle, the ideal approach to the simulation of mineral−aqueous interfaces would be to utilize the detailed surface protonation behavior, i.e., the actual acid−base reactions and water dissociation processes occurring at the mineral surface. To date, such approaches have not been applied to large molecular ensembles, due to the formidable complexity behind the atomistic description of the surface chemistry. Therefore, here we opt for a reasonable compromise between the realism of a fully atomistic description of the metal-oxide surface (as well as the aqueous electrolyte fluid phase), and the practicality of classical simulation methods based on well-characterized force fields derived from ab initio methods. Consequently, this approach provides the opportunity to fully characterize the microscopic behavior of the fluid phase in the neighborhood of the mineral surface.

We limit the current treatment mainly to neutral and negatively charged surfaces, since this effort is part of a coordinated experimental and computational study, which to date has focused primarily on the sorption of cations on the rutile surface. More specifically, our goal is to investigate the structure and reactivity of electrolyte solutions in contact with an atomistically detailed (110) rutile surface when this surface is either neutral or negatively charged. This is accomplished by choosing conditions similar to those from surface titration,[13] by aiding and assisting in the interpretation of X-ray standing wave experiments on submerged rutile (110) single-crystal surfaces,[14,15] and by providing molecular-based details of the electric double layer structure needed to clarify the surface complexation modeling results.[1,12]

In this paper, we summarize the ab initio derivation of force fields, relaxed structures, and charges of the ideal rutile (110) surface in contact with aqueous solutions,[16,17] which is the first step toward large-scale MD simulations, and introduce the interatomic potential models used to describe the (110) rutile surface, the solvent water, the ions in solution, and their corresponding interactions with one another. The SPC/E water model and the water−ion interaction potentials with SPC/E water are used exclusively in this effort, as will be explained below. We investigate four types of rutile (110) surface depending on the extent of hydroxylation and surface charge, namely, the neutral hydroxylated and nonhydroxylated surface and their negatively charged counterparts. The detailed analysis of the adsorption of ions (Rb$^+$, Na$^+$, Sr^{2+}, Ca^{2+}, Zn^{2+}, and Cl$^-$) at the interface is presented in Part 2 of this series.[34]

TABLE 1: Atomic Charges and Lennard-Jones Parameters of SPC/E Water and Ions

$$E_{ij} = 4\sqrt{\epsilon_i\epsilon_j}\left[\left(\frac{\sigma_i + \sigma_j}{2r_{ij}}\right)^{12} - \left(\frac{\sigma_i + \sigma_j}{2r_{ij}}\right)^6\right] + \frac{q_iq_j}{4\pi\epsilon_0 r_{ij}}$$

atom	q_i (e)	σ_i (Å)	ϵ_i (kcal/mol)
O	−0.8476	3.166	0.1554
H	+0.4238		
Rb$^+$	+1	3.528	0.1
Cl$^-$	−1	4.401	0.1
Sr^{2+}	+2	3.324	0.1

2. Force Field Derivation

To carry out molecular dynamics simulation of the rutile−aqueous solution interface, the interaction potentials of all species must be known. For the aqueous solution (water and dissolved ions) we employed existing models and potentials. Water was assumed to be adequately represented by the rigid, nonpolarizable SPC/E model,[18] which assigns partial charges to the oxygen, $q_O = -0.8476e$, and two hydrogens, $q_H = +0.4238e$, and applies a Lennard-Jones (LJ) potential to the oxygen site; see Table 1. This model is known to accurately reproduce the phase envelope of bulk water, as well as the liquid water structure, diffusivity, and dielectric properties over a wide range of temperature and density conditions.[19] Interaction potentials of ions dissolved in SPC/E water, given in Table 1, are available from the literature.[20,21] Having these potentials, only the interaction potentials involving the rutile surface needed to be derived.

The SPC/E model, as most water models used in simulations, does not allow for dissociation of water molecules. The development of dissociative water models does not seem to have reached the point to be applied in such large-scale simulations as those presented here, due to prohibitive computer time requirements resulting from the inclusion of three-body terms[22] or molecular orbital energies.[23] Moreover, water−ion potentials are missing for dissociative water models. Therefore we have chosen to use the SPC/E water model to be able to immediately respond to ongoing X-ray and pH titration experiments and MUSIC/SCM modeling.[24] Since a major goal of this effort is to determine the atomic-scale structure of the EDL, we further anticipate that the SPC/E model, which adequately describes bulk water and electrolyte structural and thermodynamic properties, will be useful in this context. If a dissociative model of water was used, the development of surface charge would occur naturally via formation of bonds between surface species and O and H atoms of water; that is, adsorption of surface hydroxyls modifying the surface charge. With the nondissociative model of water, we can still investigate the effect of surface charge on interfacial properties, but the surface charge has to be set explicitly via addition of charged groups (hydroxyls and hydrogens) on the surface. Having the titration results on charging of rutile as a function of pH, we are able to link the conditions of our simulations (surface charge) to pH.

The first step in modeling of the rutile surface was ab initio calculation of relaxed interfacial structure by energy minimization and derivation of the classical force fields for interactions of the surface with water molecules and ions in the aqueous solution.[16] The methods and results of this study were similar to earlier periodic density functional theory (DFT) calculations.[25] Details of the ab initio calculations for neutral surfaces are given in ref 16, and therefore the next two subsections are devoted to describing how these previous ab initio derived structures and force fields were used in our large-scale molecular dynamics

Electric Double Layer at the Rutile (110) Surface

J. Phys. Chem. B, Vol. 108, No. 32, 2004 **12051**
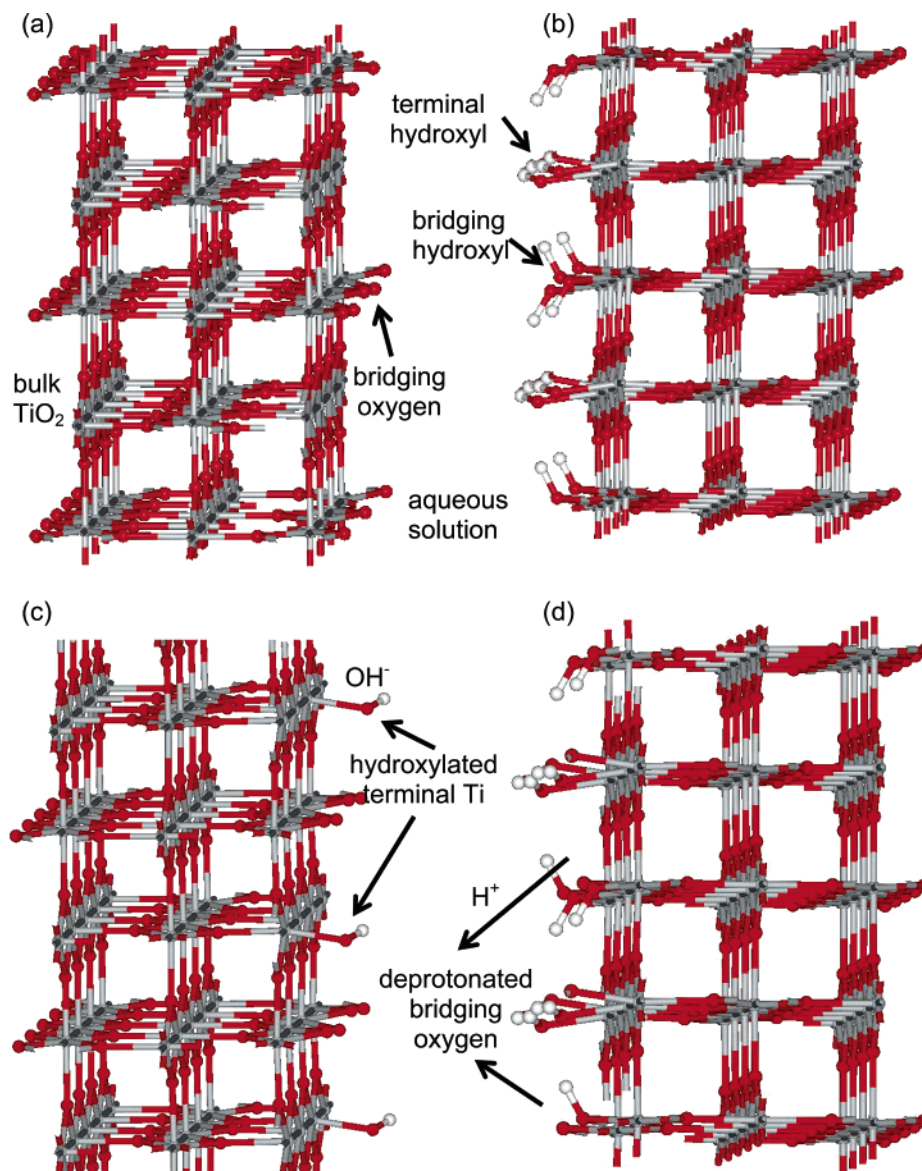
Figure 1. Structure of the neutral nonhydroxylated (a), neutral hydroxylated (b), negatively charged nonhydroxylated (c), and negatively charged hydroxylated (d) rutile (110) surfaces. The Ti atoms are shown in gray, O atoms in red, and H atoms in white. The charging of the nonhydroxylated surface by addition of terminal hydroxyls, as well as charging of the hydroxylated surface by removal of some bridging hydrogens, is indicated by arrows in panels c and d.

simulations. Also, a new ab initio-based scheme for assignment of charges on surfaces bearing net charge and its application in molecular dynamics simulations is introduced in section C.

Because spectroscopic studies of water interaction with the rutile (110) surface under vacuum conditions as well as ab initio calculations involving limited numbers of water molecules have indicated that both molecular water and hydroxyl groups exist at the surface,[26] we chose to simulate the interaction of molecular water with the aprotic, vacuum-termination (the nonhydroxylated surface), and the surface resulting from sorption of water molecules followed by their dissociation into surface hydroxyl groups (the hydroxylated surface).

A. Neutral Nonhydroxylated (110) Surface. The bulk rutile structure is characterized by 6-fold coordinated Ti atoms and 3-fold coordinated O atoms. The nonhydroxylated (110) surface stems from the relaxation of the rutile bulk structure cleaved by the (110) plane. Only rows of bridging oxygens (each bonded to two underlying Ti atoms) protrude out of the surface layer containing 5-fold coordinated titanium and 3-fold coordinated oxygen atoms (Figure 1a).

The Matsui and Akaogi[27] force field for bulk crystallographic modifications of TiO_2 was found to be the best starting point for the optimization of surface TiO_2 parameters. When the charges of surface Ti and O atoms were optimized, it was found that the original atomic charges $q_{Ti} = 2.196e$ and $q_O = -1.098e$ can be ascribed not only to Ti and O atoms in deeper layers of TiO_2 but also with success to surface Ti and O atoms. The nonelectrostatic interactions are treated in the form of a Buckingham potential (see Table 2), and these approximations provide reasonably accurate agreement between force field and ab initio structures generated by energy minimization.

The interactions between titanium atoms and the oxygens of water molecules ($Ti-O^{H_2O}$) were optimized to give the best agreement between the force field minimization and the ab initio calculations and are described by a Buckingham potential in Table 2. The optimization of the nonelectrostatic interactions between the oxygens of rutile and water revealed that it is possible to set these interactions equal to those between two water oxygens; that is, they were set equal to the O−O Lennard-Jones interactions of the SPC/E water model. Similarly, the

TABLE 2: Parameters of Buckingham Potential[a] for Interaction between Ti and O Atoms

$$E_{ij} = A_{ij} \exp(-r_{ij}/\rho_{ij}) - C_{ij}/r_{ij}^6$$

$i-j$	A_{ij} (kcal mol^{-1})	ρ_{ij} (Å)	C_{ij} (kcal mol^{-1} Å^6)
Ti−O	391 049.1	0.194	290.3317
Ti−O[b]	315 480.8	0.194	290.3317
Ti−Ti	717 647.4	0.154	121.0676
O−O	271 716.3	0.234	696.8883
Ti−O$^{\mathrm{H_2O}}$ [c]	28 593.02	0.265	148.000[d]

[a] Bulk atomic charges: $q(\mathrm{Ti}) = 2.196$, $q(\mathrm{O}) = -1.098$. See ref 27. [b] Modified potential[27] for terminal hydroxyl obtained in small hydroxide complexes. [c] Interaction between the water oxygen and Ti atom approximated by Buckingham function. [d] Value of Ti−O dispersion coefficient has been estimated from polarizabilities of Ti^{4+} ion and water molecule (see text).

nonelectrostatic interaction between rutile surface oxygens and ions in the solution was set equal to that between oxygen of bulk SPC/E water and the same ions. To our knowledge, there are no nonelectrostatic potentials available in the literature for the interaction of Ti and the ions used in our simulations; therefore, the interaction between Ti atoms and ions in the solution was taken to be purely electrostatic. This was deemed reasonable because, as will be demonstrated below, the surface titanium atoms are always shielded from direct interaction with dissolved ions by a layer of oxygen atoms. Moreover, electrostatic interactions dominate long-range interactions.

One way to approach the dynamics of the surface in MD simulations is to allow all Ti and O atoms to move and to apply Matsui and Akaogi potentials. However, we did not follow this approach since (i) it is doubtful that the resulting relaxed structure would be more accurate than the one obtained from ab initio calculations and (ii) allowing for surface dynamics greatly increases the computational demands of MD simulations. Therefore, we decided to model the neutral nonhydroxylated surface as rigid. To validate this approach, we ran a simulation in which the bridging oxygens were allowed to move within fixed bond lengths (as for the hydroxylated surface below), but the results were unaffected by the motion of bridging oxygens, which was in any case quite limited.

B. Neutral Hydroxylated (110) Surface. The fully hydroxylated surface originates from the dissociative adsorption of water on the nonhydroxylated surface. The hydroxyl group from a water molecule binds to the terminal 5-fold coordinated surface Ti atom and becomes a terminal hydroxyl. The other hydrogen from the water molecule binds to the bridging oxygen and forms a bridging hydroxyl (Figure 1b).

As for the neutral nonhydroxylated surface, the charges of surface atoms were fitted to produce the best agreement with ab initio derived structures. At the end of this exercise it was found that only the charges of terminal and bridging O and H atoms had to be modified. The resulting values are given in Table 3 (neutral hydroxylated surface). Also included in Table 3 are corresponding charges as calculated with the revised MUSIC model.[6,7] These charges are based on the formal valence of oxygen (-2) minus the bond-valence contribution from Ti atoms ($+4$ charge) coordinated to the surface oxygens, which depends on the length of the Ti−O bonds involved. Under the revised MUSIC model approach, the residual charge on the surface oxygens is balanced by hydrogen-bond formation with associated water molecules.

Due to the hydrogen bonding among bridging and terminal hydroxyl groups and water molecules, it was not possible to keep the hydroxyl groups rigid during the simulations. Moreover, the geometry of the hydroxyl groups obtained from ab initio simulations proved sensitive to the number of surrounding water molecules, which indicates that there are several favorable configurations that have to be sampled during the simulations.[17] Therefore, the bridging and terminal hydroxyl groups at hydroxylated surfaces were kept flexible during the simulation, within fixed Ti−O and O−H bond lengths averaged from the ab initio structures (see Table 4). Note that the length of the bridging Ti−O bond changes upon protonation of the bridging oxygen. An ab initio-derived bending potential for the Ti−O−H angle, $E_{\angle \mathrm{Ti-O-H}} = (1/2)k_2(\theta - \theta_0)^2$, with $k_2 = 14.136$ kcal mol^{-1} rad^{-2} and $\theta_0 = 90.85$ deg, was applied to both the terminal and the bridging hydroxyl groups, summing the contribution from both Ti atoms bonded to bridging oxygen in the latter case. In addition to this bending potential and the

TABLE 3: Charges of Surface Atoms for the Neutral Nonhydroxylated and Hydroxylated Surfaces and the Basic Charges According to the Scheme for Preparation of Charged Surfaces[a]

	neutral surface		charged surface		
atom	nonhydroxylated	hydroxylated	nonhydroxylated	hydroxylated	MUSIC model[b]
Terminal Group					
terminal Ti	2.196	2.196	**2.156**	**2.156**	4.0
3-fold coordinated O in Ti layer	−1.098	−1.098	−1.098	−1.098	−2.0
3-fold coordinated O in Ti layer	−1.098	−1.098	−1.098	−1.098	−2.0
terminal hydroxyl O		−1.008		**−0.939**	−1.254
terminal hydroxyl H		0.459		**0.430**	1.0
sum	0.000	−0.549	**−0.04**	**−0.549**	−0.254
Bridging Group					
bridging Ti	2.196	2.196	**2.156**	**2.156**	4.0
3-fold coordinated O under Ti layer	−1.098	−1.098	−1.098	−1.098	−2.0
unprotonated bridging O	−1.098		**−1.018**		−0.405
protonated bridging O		−1.035		**−0.964**	
bridging H		0.486		**0.455**	1.0
sum	0.000	0.549	**0.04**	**0.549**	0.595
Other Atoms (Bulk Atoms)					
Ti	2.196	2.196	2.196	2.196	4.0
O	−1.098	−1.098	−1.098	−1.098	−2.0
O	−1.098	−1.098	−1.098	−1.098	−2.0
sum	0.000	0.000	0.000	0.000	0.0

[a] Variable charges (shown in boldface type) are further modified by the redistribution of the remaining charge along surface atoms (see the text and Table 4). [b] Corresponding charges as defined according to the revised MUSIC Model are included for comparison. All charges are given in the unit of electron charge.

Electric Double Layer at the Rutile (110) Surface

J. Phys. Chem. B, Vol. 108, No. 32, 2004 **12053**

TABLE 4: Surface Ti−O and Ti−O−H Bond Lengths Averaged from ab Initio Structures and Used in MD Simulations[a]

bond	terminal		bridging protonated		bridging unprotonated
	Ti−O	O−H	Ti−O	O−H	Ti−O
length (Å)	1.895	0.983	2.022	0.994	1.872

[a] The length of the bridging Ti−O bond changes upon protonation of the bridging oxygen.

electrostatic interactions among all atoms, the bridging and terminal oxygens interact with all oxygen and titanium atoms of the rutile via the Matsui and Akaogi potential. All remaining interactions are the same as for the nonhydroxylated surface, including the Lennard-Jones interactions for the bridging and terminal oxygens with solution species as well as Coulombic interactions.

C. Negatively Charged (110) Surfaces. One of our primary goals is to model at the atomistic level, without introducing any homogeneous background charge density, surfaces exhibiting nonzero net charge. Particularly, the negatively charged surface was chosen in this study because surface titration studies demonstrated that aqueous ions interact much more extensively with the negatively charged surface than with either neutral or positively charged surfaces. The point of zero charge (pH_{zpc}) of rutile is about 5.4 at 25 °C[13] and thus negative surface-protonation-induced charge develops at any pH above this point. To simulate the negatively charged surface, the first possible extreme case in terms of coverage of terminal and bridging hydroxyls is a surface with no bridging hydroxyls and a selected number of terminal hydroxyls. Such a surface can be interpreted as originating from the neutral nonhydroxylated surface by conversion of some of the water molecules that naturally adsorb above the 5-fold surface Ti atoms to bonded hydroxyls. To point out the similarity of this surface to the neutral nonhydroxylated surface we term this surface the *negative nonhydroxylated surface*. The number of terminal hydroxyls determines the resulting surface charge density σ_H. The other extreme case of negatively charged surface in terms of surface hydroxyl coverage is a surface with full coverage of terminal hydroxyls and a smaller coverage of bridging hydroxyls, since the MUSIC model predicts that the bridging proton is more acidic.[6,7] This surface can be obtained from the neutral hydroxylated surface by removal of some of the bridging hydrogens and we term it the *negative hydroxylated surface.* In this case, it is the number (percentage) of unprotonated bridging oxygens that determines the surface charge density.

All atoms participating in hydrogen bonding, i.e., terminal and bridging oxygen and hydrogen atoms, were allowed to move within fixed bond lengths as in the case of the neutral hydroxylated surface. All other atoms of the negative hydroxylated surface were kept fixed in the relaxed ab initio positions of the neutral hydroxylated surface, since the deprotonation of bridging oxygen had little effect on the positions of other atoms. Similarly, the ab initio relaxed structure of the neutral nonhydroxylated surface was adopted for all rigid atoms at the negative nonhydroxylated surface except the hydroxylated terminal Ti atoms. Ab initio calculations reveal that while the bare terminal Ti atom is relaxed by about 0.1 Å inward, when it is hydroxylated its relaxation with respect to the ideal crystal geometry is zero. The positions of hydroxylated terminal Ti atoms at the negative nonhydroxylated surface were therefore kept with zero relaxation.

We have imposed the realistic condition that the adsorption of a terminal hydroxyl group must decrease the surface charge

by 1e and protonation of bare bridging oxygen increases the surface charge by 1e. However, because the ab initio oxygen and hydrogen surface charges are lower than their nominal charges ($-2e$ and $+1e$, respectively), nearly by a factor of 2, removal/addition of these species cannot result in a change in surface charge of $\pm 1e$, and consequently the redistribution of the remaining charge among neighboring surface atoms must take place.

Quantum mechanical calculations[16] of the hydroxylated surfaces confirm that total charge of terminal and bridging hydroxyl groups never reaches $\pm 1e$ and that the negative or positive charge is spread among the surrounding atoms. Because of this, we devised a scheme for the assignment of the charges to negatively charged surfaces that is also based on an ab initio calculation of partial charges for O and H in small titanium hydroxide clusters[17] and takes into account the qualitative results of Mulliken population analysis[16] for hydroxylated surfaces.

According to this scheme, the CHelpG charges on oxygen and hydrogen in small titanium clusters were scaled such that the average CHelpG charge on H atoms of water molecules (within these systems) became equal to their values in SPC/E model water. The Ti, O, and H atoms of terminal and bridging groups are variable-charge atoms. Their basic charges, which these atoms would adopt for neutral surfaces, are given under the heading "charged surface" in Table 3. In the case of charged surfaces, the missing charge, arising from the difference between nominal and actual charges of hydroxyl groups, distributes between the variable-charge atoms equally. This scheme can be applied to all surfaces including neutral ones, for which it gives slightly different surface charges than those given in the preceding two subsections. For MD simulations of neutral surfaces, we used the surface charges as given in the preceding two subsections and under the heading "neutral surface" in Table 3, because these parameters were obtained and used in MD simulations prior to our work on charged surfaces and before the present charging scheme was devised. We have checked that both sets of charges yield very similar results. Therefore, the charging scheme can be applied with confidence for both neutral and negative surfaces.

Because of the redistribution of the missing charge among variable-charge atoms, the charges of these atoms depend on the coverage of the surface by hydroxyl groups of both kinds or, in other words, on the surface charge density. The maximum charging of the surface would yield a surface charge density (there are two hydroxyl/bridging groups in the ab initio cell) $2(-1e)/(5.918 \times 6.497 \text{ Å}^2) = -0.83$ C/m^2, which is considerably more negative than the observed surface charge density σ_H developed on rutile powder suspensions in 0.03−1.0 *m* NaCl solutions at 25 °C and pH = 11.[13] We extensively simulated charged surfaces with surface charge density −0.208 C/m^2 (25% of maximum charge density). We have also performed a few simulations with surface charge density −0.104 C/m^2. The corresponding pH values for which these surface charge densities develop are about 10 and 8, respectively, in NaCl solutions at room temperature.[13] The final charges for the two surface coverages studied are given in Table 5. As the surface charge density decreases, the missing charge is distributed among more atoms, and the resulting atomic charges become closer to those given in Table 3 for the situation where there is a balance between the number of terminal and bridging hydroxyls. The geometric distribution of the net-charge-determining species along the surface for both surface coverages is shown in Figure 2. When this scheme was devised, the pattern

TABLE 5: Resulting Charges of the Variable-Charge Surface Atoms Based on the Scheme for Two Surface-Charge Densities

atom	negative nonhydroxylated		negative hydroxylated	
	$\sigma_H = -0.208$ C/m^2	$\sigma_H = -0.104$ C/m^2	$\sigma_H = -0.208$ C/m^2	$\sigma_H = -0.104$ C/m^2
5- and 6-fold coordinated Ti	2.121	2.137	2.134	2.146
terminal hydroxyl O	−0.974	−0.956	−0.960	−0.949
terminal hydroxyl H	0.394	0.412	0.409	0.420
unprotonated bridging O	−1.053	−1.037	−1.039	−1.028
protonated bridging O			−0.985	−0.976
bridging H			0.434	0.444
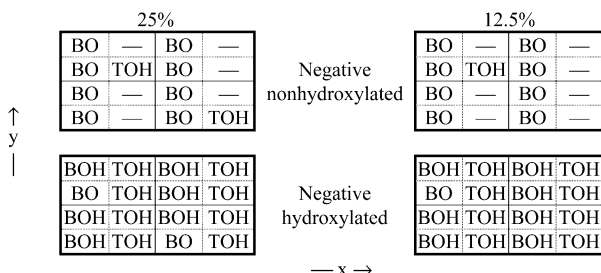
Figure 2. Geometric scheme of the distribution of surface groups forming 25% coverage (left) and 12.5% coverage (right) of charged groups for both negative surfaces. BO, unprotonated bridging oxygen; TOH, terminal hydroxyl; —, bare 5-fold coordinated Ti atom; BOH, bridging hydroxyl. The thin solid lines separate elementary ab initio structures.

allowing maximum separation of like-charged groups was considered, thus minimizing Coulombic repulsion.
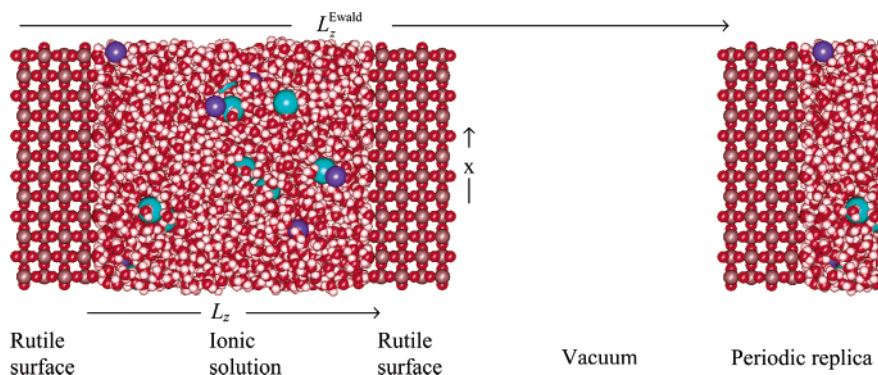
3. Molecular Dynamics Simulation

To obtain the structure of the rutile−aqueous solution interface, we performed molecular dynamics simulations of a slab geometry system with two parallel TiO$_2$ walls and water molecules (and ions, if present) between them. Therefore, this system has two identical interfaces (both surfaces hydroxylated or both nonhydroxylated) and the properties reported are averages over both interfaces. A snapshot of the simulation cell is shown in Figure 3.

The structure of each of the surfaces was created by periodic replication of the elementary ab initio cell of dimensions $l_x =$ 5.918 Å and $l_y =$ 6.497 Å containing four surface Ti atoms, four surface oxygen atoms, and two bridging oxygens for nonhydroxylated surface, and for the hydroxylated and charged surfaces, additional terminal hydroxyls and bridging hydrogens. The surface structure was extracted from the relaxed ab initio structure of the five-layer slab, taking three layers from one side including the central, unrelaxed layer. In the molecular dynamics simulations we applied a cutoff distance $R_c = 12.66$ Å for all real-space interactions, so one more unrelaxed layer

was added to the surface structure to make it sufficiently wide for this cutoff distance. The two interfacial layers of the resulting four-layer TiO$_2$ surface are thus relaxed and the two farther from the interface have the ideal bulk crystal geometry. Neutral relaxed ab initio structures (either nonhydroxylated or hydroxylated) were used for rigid atoms, and Ti−O and O−H bond lengths determined from neutral structures (Table 4) were used for dynamics of flexible atoms. The charges of the surface atoms were fixed to those given in Table 3 for neutral surfaces and Table 5 for negative surfaces.

The lateral size of the MD simulation box was $L_x = 6l_x =$ 35.508 Å and $L_y = 6l_y =$ 38.981 Å; that is, the quantum cell was replicated six times in both x and y directions, where periodic boundary conditions were used. The separation of the two surfaces in the slab, L_z, measured between the layers of surface Ti atoms as if they were not relaxed, was adjusted to yield the desired density and pressure in the bulklike phase in the middle of the slab. The separation L_z of the two surfaces, $L_z \approx 50$ Å, is large enough to establish bulklike water in the center of the slab and to prevent the interference of the two surfaces. It turns out that the interfacial region spans across about 15 Å at each of the surfaces, leaving still about 20 Å of bulk region in the center of the slab.

The neutral nonhydroxylated surface was simulated with 2048 water molecules. From this number, 144 water molecules are observed to associatively adsorb on the surface above each of the terminal Ti sites, and these water molecules are essentially immobile. However, there is no difference in the modeling of the adsorbed and other water molecules; all are treated with the SPC/E model. For the charged and hydroxylated surfaces, the number of associated water molecules is 2048 less the number of dissociatively adsorbed water molecules, which become the terminal hydroxyl and protonated bridging oxygen sites. In this way, the number of oxygens and hydrogens is identical for both nonhydroxylated and hydroxylated surfaces. In this paper we concentrate on the properties of water at the interface only (the properties of ions are the subject of Part 2

Figure 3. Geometry of the molecular dynamics periodically replicated simulation cell in x and y directions with indicated additional periodicity in z direction for calculation of electrostatic interactions by use of Ewald sum. O (red), Ti (grey), and H (white) atoms are scaled down for clarity; Rb (blue) and Cl (cyan) ions are shown in actual size.

Electric Double Layer at the Rutile (110) Surface

J. Phys. Chem. B, Vol. 108, No. 32, 2004 **12055**

in this series[34]); therefore, the results for the neutral surfaces were obtained for pure water between the interfaces.

To converge long-range electrostatic interactions, the total simulation box has to be neutral. Therefore, to simulate negatively charged surfaces, the negative surface charge has to be counterbalanced by a surplus of cations in the solution. For this purpose, we dissolved 48 Rb^+ ions and 12 Cl^- ions, or 27 Sr^{2+} ions and 18 Cl^- ions, in the solution, which compensates the total negative charge of $-36e$ of the two identical surfaces of the simulation cell at $\sigma_H = -0.208$ C/m^2. Comparing the results for either Rb^+ or Sr^{2+} ions being present, we verified that the structure of water is unaffected by the choice of cation and is rather a property of the charged surface itself.

A three-dimensional Ewald sum with correction for the 2D periodic geometry, EW3DC,[28] with $K_{max} = 5$ and vacuum gaps between replicas as wide as the system wall−water−wall, was verified to account accurately for the long-range electrostatic interactions. We checked that the width of the gap must be at least 20% of the width of the wall−water−wall system (which is about 70 Å) for the method to work; enlarging the gap width to 50% already produces quite accurate results, and using a gap as wide as the studied system (which we did) shows no dependence of the atomic forces on the gap width, i.e., we are effectively reaching the limit of infinite gap separation with no z periodicity. We emphasize that even in this limit the EW3DC method is not identical to the standard 3D Ewald method applied to systems with 3D periodicity, because of a different shape-dependent term in the Ewald sum, which guarantees better convergence.

A fourth-order predictor−corrector and the quaternion formalism were used for dynamics and keeping the rigid geometry of water molecules. The motion of surface hydroxyl groups of the hydroxylated surface was governed by the Verlet algorithm with SHAKE to maintain the fixed bond lengths.

The time step of 1.2 fs was applied. Following at least 100 000 equilibration steps, at least 800 000 MD steps were performed, resulting in simulation time of 1 ns. In fact, reliable data on water structure are obtained from runs as short at 200 000 cycles.

4. Results

A. Interface Structure. We have performed simulations at ambient conditions, $T = 298.15$ K and $\rho_{bulk} = 1$ g/cm^3, and at $T = 448$ K and $\rho_{bulk} = 0.9$ g/cm^3, reflecting the density of water in equilibrium with its vapor at each temperature. We will discuss only the room-temperature results in detail since the influence of temperature on interfacial structure proved to be very small. Unlike in a vacuum, the relaxation of the rutile surface in contact with aqueous solution is minimal, with the displacement of surface Ti atoms being less than about ±0.1 Å. This is fully consistent with X-ray crystal truncation rod studies of rutile (110) single-crystal surface in contact with liquid water at room temperature.[24] The heights of surface atoms from ab initio calculations and MD are given in Table 6. The agreement between ab initio and MD positions of terminal and bridging oxygens is guaranteed by use of ab initio bond lengths for corresponding Ti−O distances, as given in Table 4. The zero height is set to the position that the surface layer of Ti atoms would occupy in the unrelaxed crystal termination. This definition is identical for both hydroxylated and nonhydroxylated surfaces despite the different relaxation of these surfaces. The reason for this convention is to allow direct comparison with the positions of surface and solution atoms obtained from X-ray experiments, which are relative to the (110) d spacing of the bulk crystal, as discussed in Part 2 of this series.[34]

TABLE 6: Heights of Atoms in the Interfacial Layer of Relaxed (110) Surface Including Terminal Oxygens or Adsorbed Water Molecules[a]
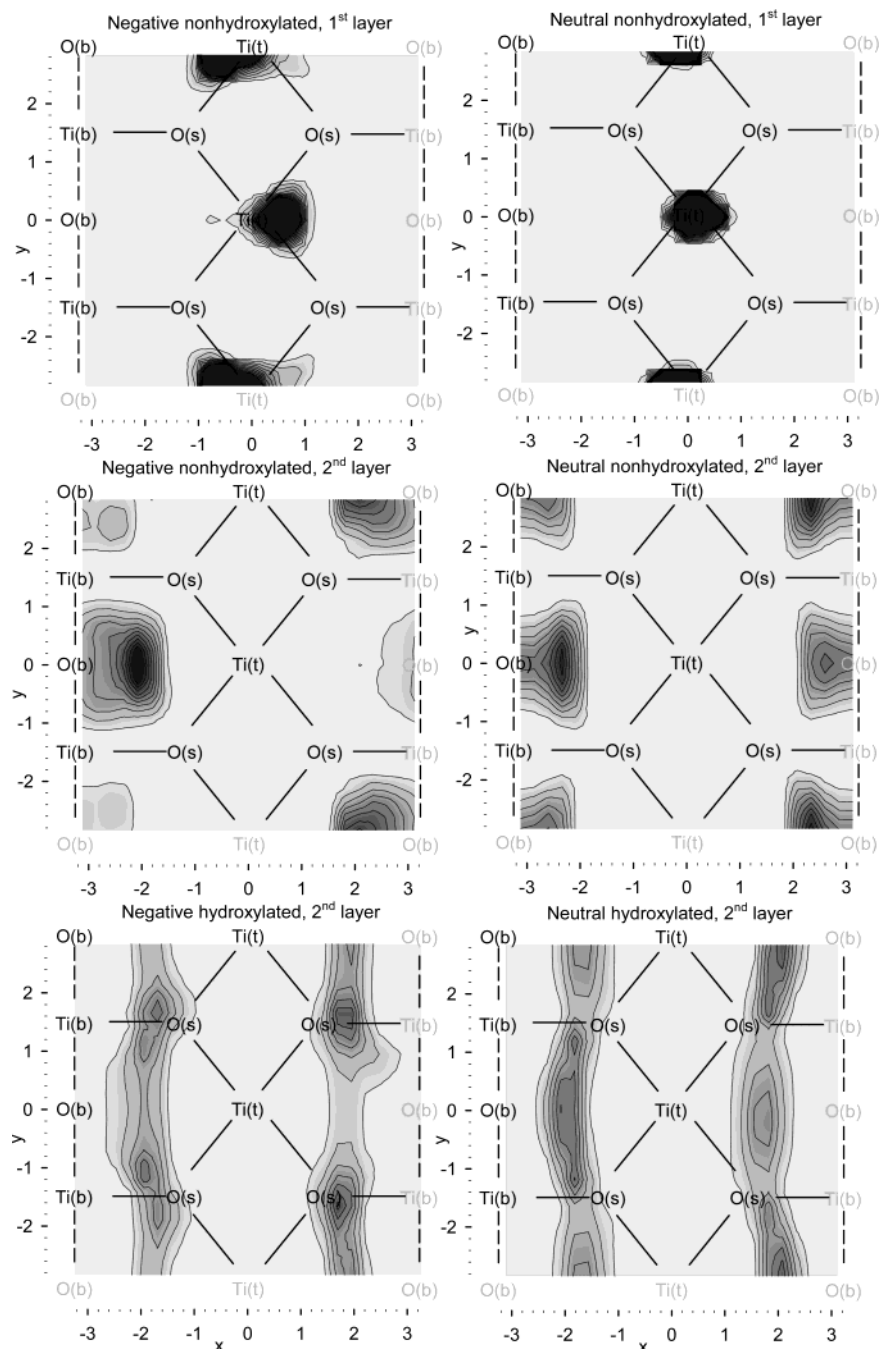
atom	nonhydroxylated surface	hydroxylated surface
bridging Ti	0.13	0.005
unprotonated bridging O	1.27	
	1.25 ± 0.05	1.13 ± 0.05[b]
protonated bridging O		1.38
		1.36 ± 0.05
hydroxylated terminal Ti	0.13[b]	0.12
nonhydroxylated terminal Ti	−0.09	
associated terminal H$_2$O	2.15[c]	
	2.20 ± 0.1[c]	
	2.37 ± 0.1[b]	
terminal O		1.99
	2.0 ± 0.05[b]	1.97 ± 0.05

[a] Ab initio heights are given as numbers only; heights from molecular dynamics simulations are given with error ranges. Titanium atoms are treated as immobile in MD. [b] Data for negatively charged surface only. [c] Data for neutral surface only.
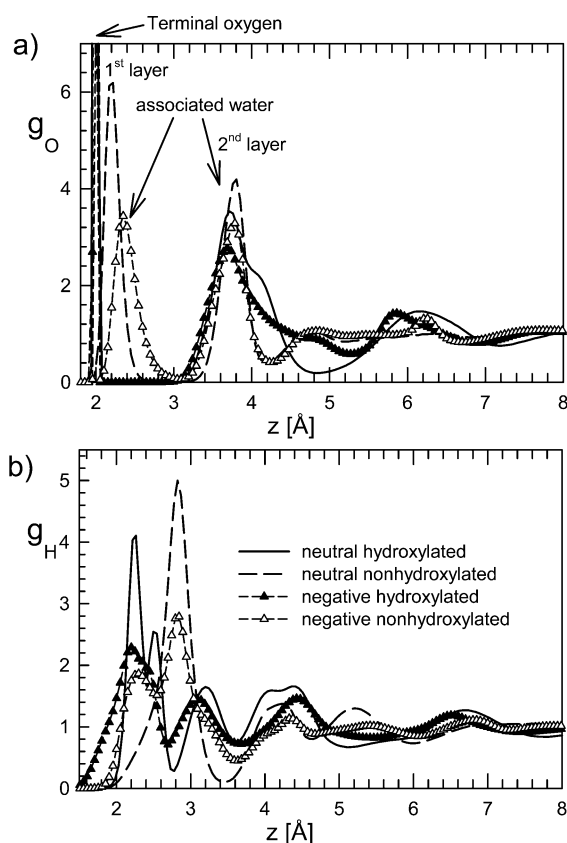
Figure 4. Axial density profiles of oxygen (top) and hydrogen (bottom). The sharp peak at 2.0 Å corresponds to terminal oxygen; the positions of the oxygen of adsorbed water molecule above bare Ti^V are 2.2 and 2.35 Å for the neutral and negatively charged nonhydroxylated surface, and the height of second-layer adsorbed water molecules is 3.7−3.8 Å for all surfaces. At further distances, the structuring of water is minimal for neutral surfaces and pure water, while for negative surfaces, structuring of water is observed due to the presence of ions.

The density profiles of oxygen and hydrogen are compared in Figure 4 for all four types of surface. The density profile shows the average density of atoms of a given kind as a function of distance from the surface, and the normalization was chosen such that the unit corresponds to the water density of 1 g/cm^3. The axial profiles give information on the height of oxygens above the Ti surface plane but provide no information on the lateral position of oxygens relative to the structured surface. To be able to analyze the adsorption sites of water molecules

Figure 5. Contour plots of the lateral density profiles of water molecules in the first layer (top row) and second layer (middle row) at nonhydroxylated surface and in the second row at hydroxylated surface (bottom row). The differences between negative surfaces (left column) and neutral surfaces (right column) are marginal. The first layer of interfacial oxygens at the hydroxylated surface is formed by terminal hydroxyls, which prevent water molecules from occupying their place. Contours are shown in increments of unit reduced density, which corresponds to a uniform distribution. Darker color means higher density.

at the surface, we have calculated the lateral density profiles of oxygen atoms at narrow bins of width $\Delta z = 0.1$ Å. In this way, the density of oxygen atoms as a function of lateral coordinates x and y is recorded at different heights above the surface, providing a three-dimensional density map of water molecules. From this more detailed information, the lateral density profiles in a selected layer (height) above the surface can be easily obtained by integration over the range of z coordinate. In Figure 5 we plot the lateral density profiles of water molecules in the first and second layers at the nonhydroxylated surface and in the second layer at the hydroxylated surface.

The axial profile of oxygen (Figure 4) shows two distinct peaks at distances 1.9−2.4 Å and around 3.8 Å. The first peak

corresponds to the first layer of adsorbed oxygens, which are either the terminal hydroxyls present on all surfaces except the neutral nonhydroxylated, giving rise to the sharp peak at 2.0 Å, or molecularly adsorbed water molecules in the terminal site, giving rise to a peak at 2.2 Å at the neutral nonhydroxylated or 2.35 Å for the negative nonhydroxylated surface. The latter separation distance is larger because of the electrostatic repulsion between water molecule oxygens and the negatively charged surface. The length of the Ti−O bond for terminal hydroxyl groups is fixed to 1.8949 Å (see Table 4), and the peak of terminal hydroxyl oxygens at 2.0 Å indicates that the Ti−O bond is perpendicular to the surface. X-ray experiments[24] cannot distinguish terminal oxygens (part of terminal hydroxyl) from

Electric Double Layer at the Rutile (110) Surface

J. Phys. Chem. B, Vol. 108, No. 32, 2004 **12057**

TABLE 7: Positions of Oxygen Peaks and Numbers of Protonated/Unprotonated Bridging Oxygens and Terminal Hydroxyls for All Surfaces

surface	no. of unprotonated bridging O	no. of protonated bridging OH	no. of terminal OH	no. of associated terminal H_2O	first O peak (Å)	second O peak (Å)
nonhydroxylated neutral	144	0	0	144	2.2	3.8
nonhydroxylated negative	144	0	36	108	2.0^a, 2.4	3.6
hydroxylated neutral	0	144	144	0	2.0^a	3.8
hydroxylated negative	36	108	144	0	2.0^a	3.7

[a] Position of terminal hydroxyls in the first layer.

oxygens of adsorbed water molecule above terminal Ti and give only the observed average height of 2.12 ± 0.02 Å, which lies between our MD determined heights for both oxygen species and is therefore consistent. There is excellent agreement in the height of the second layer of water molecules, 3.8 Å, between MD and X-ray experiments.[24]

The first peak of molecularly adsorbed water occurs only for nonhydroxylated surfaces, because these water molecules occupy the site above the terminal Ti atom (top row of Figure 5), which is occupied by full coverage of terminal oxygens on the hydroxylated surfaces. Counting both terminal oxygens and water molecules, the coverage of the first layer at 1.9−2.4 Å is exactly one water molecule per terminal Ti, i.e., full coverage. As will be confirmed below, the molecularly adsorbed water molecules in this layer have zero diffusion within the time frame of simulation. Consequently, the molecules are truly adsorbed, though there is no a priori restriction imposed on their dynamics—these molecules interact as any other water molecule. The second peak around 3.8 Å corresponds to water molecules interacting with the first layer of terminal and bridging oxygens; the relative coverage of this layer (divided by the number of bridging Ti atoms) is 1.0 for the nonhydroxylated surface and 1.5 for the hydroxylated surface. There is a small third peak around 4.8 Å followed by a flat density profile for nonhydroxylated surfaces. At hydroxylated surfaces, structuring of water is more pronounced up to distances 8−10 Å from the surface, with an additional oxygen peak at about 6 Å. The numbers of different types of oxygens on each type of surface and the location of corresponding peaks are summarized in Table 7. The heights of the bridging oxygens are about 1.25 Å when unprotonated and 1.4 Å when protonated (according to different Ti−O bond lengths; see Table 4 and Table 6).

The differences in lateral distribution of oxygens (Figure 5) between neutral surfaces and negative surfaces are marginal. The distribution of second-layer water molecules at the non-hydroxylated surface reveals the most probable position above the bridging oxygen is tilted toward the terminal Ti, and the preferred position above the hydroxylated surface is rather similar, only extended somewhat in the y direction parallel to rows of terminal Ti.

To understand the axial distribution of hydrogens shown in Figure 4b, it is useful to look at the angular distribution of water molecules at the same time. In Figure 6, the average cosine of the angle between the water molecule dipole vector and the inward (pointing toward the bulk water) surface normal is plotted as a function of distance from the rutile surface; thus, a positive number means a water molecule is pointing its hydrogens away from the surface. First-layer water molecules at nonhydroxylated surfaces point their dipoles away from the surface, in fact nearly perpendicularly for the neutral surface, giving rise to the hydrogen peak around 2.8 Å. This can be interpreted in terms of Ti−O attraction and the possibility of the hydrogens facing the liquid to form H-bonds with water molecules of the second layer. Indeed, the orientation of second-layer water molecules
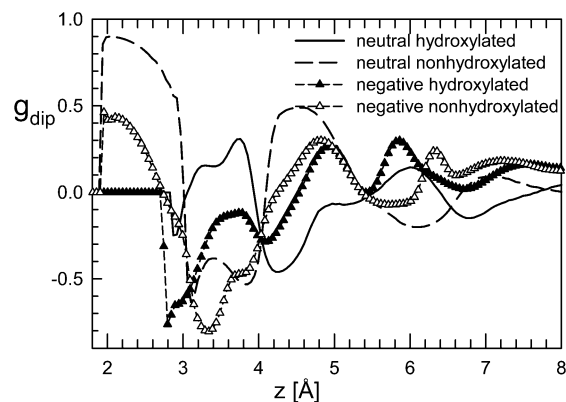

Figure 6. Average cosine of the dipole vector with the inward (pointing toward the bulk water) surface normal. Because of the nearly zero density of water molecules in the region 2.6−3.2 Å, the behavior of the lines in this region is not significant.

at nonhydroxylated surfaces is reversed; they point toward the surface. As a result, there is a broad peak of hydrogens between the first and second oxygen peaks with a relative coverage about 3, that is, containing both hydrogens of the first-layer water molecules and half those of the second layer. For the negative nonhydroxylated surface, hydrogens of the first-layer water molecules still form the peak at 2.8 Å, but some of them also contribute to the smaller peak at 2.3 Å, which coincides with the position of terminal hydroxyl hydrogens.

For the neutral hydroxylated surface, bridging hydrogens (hydrogens of bridging hydroxyls) contribute to the peak at 2.2 Å and the terminal hydrogens to the peak at 2.5 Å, while the peak at 3.2 Å is formed by one of the hydrogens of second-layer water molecules. When the hydroxylated surface is negatively charged, these positions shift by 0.1 Å closer to the surface. The difference between nonhydroxylated and hydroxylated surfaces, namely, the difference between two hydrogens being part of a water molecule or part of two surface hydroxyl groups, is most noticeable in the distribution of hydrogens at a distance of about 2.8 Å, i.e., between the first and second oxygen layers. These differences lead also to a different orientation of water molecules in the second layer of oxygens around 3.8 Å at both surfaces (Figure 6). Unlike at the nonhydroxylated surface, where these molecules point toward the surface to make hydrogen bonds with molecularly adsorbed first-layer water, the water molecules forming the second layer at the neutral hydroxylated surface tend to be oriented rather away from the surface. The negative hydroxylated surface, which has a tendency to repel oxygens and attract hydrogens, favors the molecules at the negative hydroxylated surface to be aligned toward the surface, but the average cosine of the dipole orientation of the second-layer water molecules is still close to zero.

B. Electrostatic Properties. From the axial density profiles, the charge density profile $\rho_q(z) = \sum_{i \ni surf} \rho_i(z)q_i + \rho_O(z)q_O + \rho_{H^-}(z)q_H$ is obtained as a sum of the contributions from surface

12058 *J. Phys. Chem. B, Vol. 108, No. 32, 2004*

Předota et al.
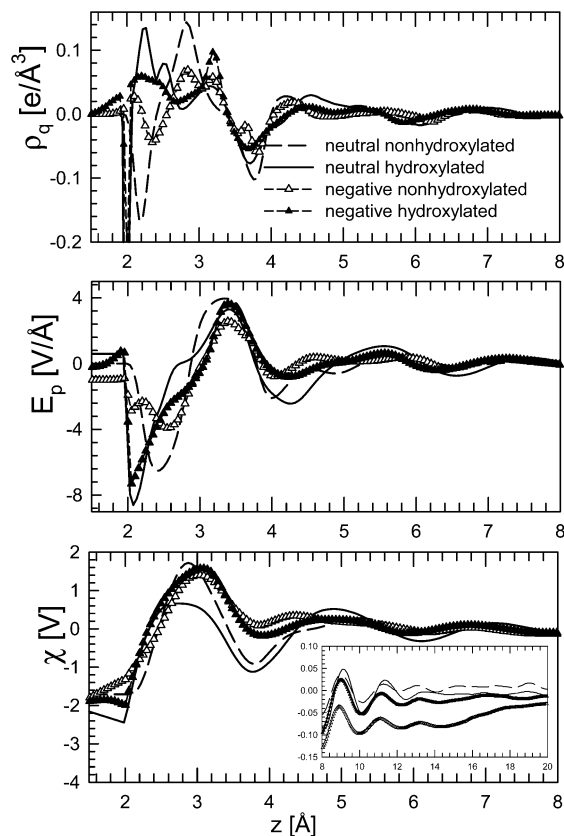
Figure 7. Electrostatic properties as a function of distance from the TiO$_2$ surface at ambient conditions: charge density ρ_q (top), electric field E_p (center), and electrostatic potential χ (bottom, with inset showing long-range oscillations and decay). The electrostatic potential has been shifted to zero in the center of the slab in all cases.

Figure 8. Axial density profiles of oxygen (a) and hydrogen (b) at negative surfaces, showing the minimal effect of increase of temperature from room temperature to 448 K (175 °C) on the interfacial structure of water.

atoms (both flexible and rigid), water oxygens, and hydrogens, respectively. Subsequently, the electric field $E_p(z) = (1/\epsilon_0) \int_{-\infty}^{z} \rho_q(z') \, dz'$, where ϵ_0 represents the vacuum permittivity and the electrostatic potential $\chi(z) = -(1/\epsilon_0) \int_{-\infty}^{z} \rho_q(z')(z - z') \, dz'$, can be calculated. The profiles of electrostatic properties are shown in Figure 7. Despite the differences in density profiles of O and H, the charge density profiles for hydroxylated and nonhydroxylated surfaces differ only at distances less than approximately 3.2 Å from the surface, as a consequence of the different structure of hydrogens at that range. At larger separations, the charge density, as well as the integrated quantities, E_p and χ, show the same features for both surfaces. Moreover, the effect of the surface negative charge is not dramatic. The electrostatic potential reveals large oscillations of the order of a few volts within 6 Å of the surface, followed by damped oscillations (see Figure 7 inset) up to about 15 Å. Note that the electrostatic potentials have been shifted in all cases to zero in the center of the slab to show the difference in electrostatic potential between bulk and interfacial regions.

One of the goals of this effort was to make a link between our MD predictions of the electrostatic potential in the interface and experimentally measured ζ potentials.[29] Traditionally, the ζ potential is assumed to be the difference in electrostatic potential at a shear plane between relatively immobile and mobile layers of water adjacent to the solid surface. In our MD simulations, based on the information from the density and electrostatic profiles and angular orientation, we see a strong effect of the surface up to distances of about 6 Å. However, no sharp distinction between immobile and mobile layers can be
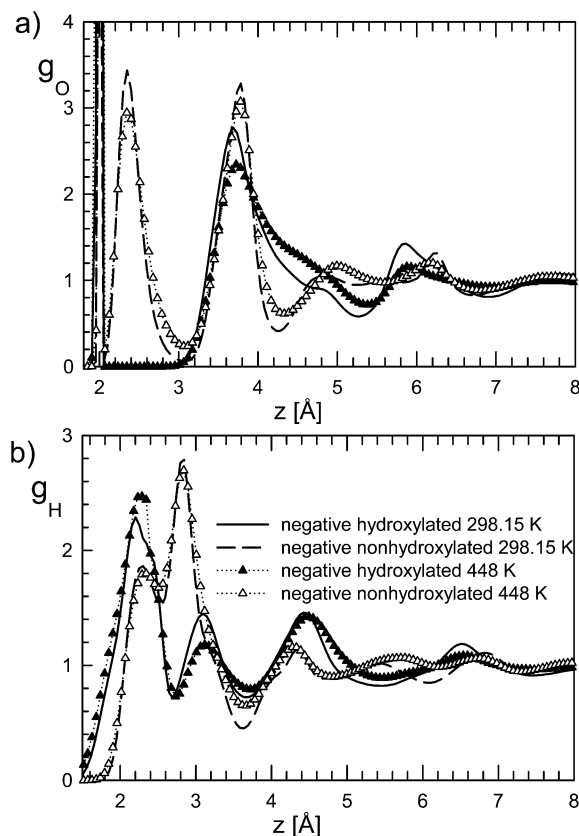
made, except for the first adsorbed layer of water molecules. Because of the observed oscillation of the electrostatic potential, predicting ζ potentials for comparison to experimental measurements[29] is not possible at the current level of simulation information gathered. Nevertheless, our simulations do not appear to indicate an extensive region (tens to hundreds of angstroms) of hindered solvent motion or structural modification, as is implied by the mathematical relationships used to derive the ζ potential from electrophoresis studies of oxide particle suspensions in water, and other electrokinetic techniques.

C. High-Temperature Interfacial Structure. Titration data of rutile powder suspensions in high-temperature NaCl solutions (up to 523 K along the liquid−vapor saturation surface[7]) indicate a substantial decrease in the pH of zero net surface charge with increasing temperature, as well as a significant increase in surface charge density for a given temperature, bulk solution ionic strength, and pH, relative to the pH of zero net surface charge at that temperature. Our molecular dynamics results for the rutile−solution interface at $T = 448$ K and $\rho_{bulk} = 0.9$ g/cm^3 indicate that the interfacial structure of water is hardly affected by the increase of temperature, as confirmed by Figure 8, where the axial density profiles of O and H atoms are compared at negative surfaces for 298.15 and 448 K. The profiles of charge density, electric field, and electrostatic potential that result from the axial profiles of O and H are therefore also insensitive to this temperature increase accordingly, as is the orientation of water molecules. This observation has important implications for the interpretation of SCM model parameters obtained from fits to pH titration and electrokinetic studies of oxide powder suspensions at elevated temperatures, particularly with regard to the dielectric properties of the solvent in the interfacial region.[7]

Electric Double Layer at the Rutile (110) Surface

J. Phys. Chem. B, Vol. 108, No. 32, 2004 **12059**
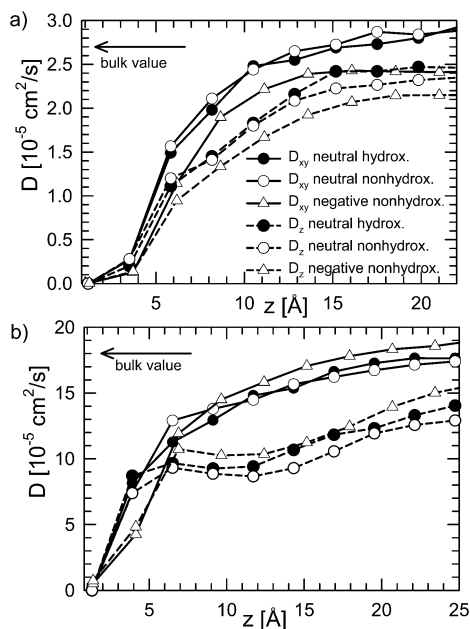
Figure 9. Perpendicular (D_z) and parallel (D_{xy}) diffusion coefficient calculated in 2.3 Å wide bins as a function of distance from the surface at $T = 298.15$ K (a) and $T = 448$ K (b). The bulk values are indicated by arrows.

D. Water Diffusivity. To quantify the dynamics of water molecules and help in identifying the mobile and immobile layers, the z-dependence of the diffusivity is plotted in Figure 9. The charging of the surface has a small effect on water diffusivity, and it is rather the effect of increasing ionic concentration that decreases the diffusivity due to reduced mobility of water molecules bonded to adsorbed ions. The diffusion constant of a homogeneous isotropic fluid is calculated as $D = \lim_{t \to \infty} \frac{1}{6} \, d/dt \, \langle [r_i(t) - r_i(0)]^2 \rangle$, where the averaging is over all molecules and time origins. In our system, we distinguish the diffusivity along the surface, i.e., in the xy plane, $D_{xy} = \lim_{t \to \infty} \frac{1}{4} \, d/dt \, \langle [x_i(t) - x_i(0)]^2 + [y_i(t) - y_i(0)]^2 \rangle$, and the diffusivity perpendicular to the surface, $D_z = \lim_{t \to \infty} \frac{1}{2} \, d/dt \, \langle [z_i(t) - z_i(0)]^2 \rangle$. Moreover, we average these diffusivities over molecules in bins parallel to the wall, to see their dependence on the distance from the surface. If a molecule is found at time t in a different bin than it was at time 0, half of the square displacement is added to the sums in the initial and terminal bins. We calculated the slope of the mean square displacement for times between 10 and 20 ps. During this time, the molecules diffuse about 3 Å from the origin, which is comparable with the width of our bins used to measure diffusion coefficients, i.e. 2.3 Å. This alleviates the issue of molecules crossing bins, effectively including partial contribution from the nearest neighboring bins only. Thanks to the selected time range for which the diffusivity was recorded, even the perpendicular mean square displacement shows linear behavior, though the long-range limit of its slope is of course zero because of the finite slab geometry of our system.

Figure 9 shows that the diffusion coefficients are insensitive to the surface hydroxylation; curves for hydroxylated and nonhydroxylated surfaces coincide within uncertainties. We confirm that the first layer of water molecules, immobile by definition for the hydroxylated surface (since it is formed by bonded terminal hydroxyls), is indeed immobile when molecular adsorption occurs. The mobility of the second layer of water molecules (around the second peak of oxygen density profile

at 3.8 Å) is about 10% of the bulk value at room temperature, and the diffusivity grows quickly in layers further from the surface, reaching the bulk value of SPC/E water, 2.7×10^{-5} cm²/s,[30] 15 Å from the surface. The experimental value of real water diffusivity at 300 K is 2.33×10^{-5} cm²/s.[31] The agreement between this value and that for SPC/E water is superior to the majority of existing water models, considering that the models are typically fitted to thermodynamic but not transport properties. The diffusivity in the z-direction is always smaller than that in the xy directions but follows the same trend. While the interfacial structure at 448 K is very similar to that at room temperature, bulk diffusivity at the higher temperature (Figure 9b) is about 6 times larger and is more steeply approached as a function of distance from the surface, with second-layer water molecules acquiring 50% of bulk diffusivity. The experimental value of bulk diffusivity at 448 K, about 1.8×10^{-4} cm²/s, is reproduced by our MD simulations.

Conclusion

The recently developed force field for interactions of water molecules with the (110) neutral rutile surface has been generalized for modeling of charged surfaces by devising a charging scheme for assignment of surface atom charges on negatively charged surfaces. This force field, as well as the bond lengths obtained from ab initio calculations for surface hydroxyls and relaxed structures of other surface atoms, has been utilized in molecular dynamic simulations of the rutile−water interface that incorporate this atomistic description of the rutile surface. The structure of water at the interface, including axial and lateral density profiles, has been analyzed. It was found that the structure of oxygens at the surface is very similar for both nonhydroxylated and hydroxylated surfaces, although molecular and dissociative adsorption take place at these surfaces, respectively. In both cases the first-layer oxygens occupy a site 1.9−2.4 Å above the terminal Ti atom and the second layer of water molecules is found at about 3.8 Å. These results are in excellent agreement with in situ X-ray crystal trunca-tion rod (CTR) measurements of rutile (110) single-crystal surfaces in liquid water at room temperature.[24] This agreement validates the choice of a nondissociating, rigid, nonpolarizable water model that is computationally efficient yet yields real-istic structural results both for bulk solutions and, as demon-strated in this study, at solid/solution interfaces down to subatomic length scales. A surprising outcome is the lack of a significant temperature effect on the interfacial structure and electrical properties, though this has yet to be experimentally validated.

We have also calculated the diffusivity profile of water molecules, which demonstrates that the first-layer water mol-ecules are immobile, but the bulk diffusivity is approached about 15 Å from the surface. We have not observed any sharp boundary between so-called immobile and mobile layers, traditionally used in interpretation of electrokinetic measure-ments. Consequently, we were not able to pinpoint a well-defined location on our axial profile of electrostatic potential at the interface, which could be linked to the experimentally observed ζ potential. Further work on model systems, including dynamic MD simulations of interfaces involving shear flow, will be necessary to study this problem. For all properties, we see little or no effect of the interface beyond 15 Å from the surface, which is in contrast to model parameters obtained from fitting some experimental electrokinetic data[29] but agrees with findings of X-ray experiments[24] and other studies.[32,33]

References and Notes

(1) Stumm, W. *Chemistry of the Solid–Water Interface*; John Wiley & Sons: New York, 1992.

(2) Blesa, M. A.; Weisz, A. D.; Morando, P. J.; Salfity, J. A.; Magaz, G. E.; Regazzoni, A. E. *Coord. Chem. Rev.* **2000**, *196*, 31.

(3) Parks, G. A. *Mineral–Water Interface Geochemistry*; Hochella, M. F., Jr, White, A. F., Eds.; Reviews in Mineralogy *23*; Mineralogical Society of America: Washington, D.C., 1990; p 133.

(4) Schindler, P. W.; Stumm, W. *Aquatic Surface Chemistry: Chemical Processes at the Particle–Water Interface*; Stumm, W., Ed.; Wiley: New York, 1987; p 83.

(5) Hiemstra, T.; Van Riemsdijk; Bolt, G. H., W. H., *J. Colloid Interface Sci.* **1989**, *133*, 91.

(6) Hiemstra, T.; Venema, P.; van Riemsdijk, W. H. *J. Colloid Interface Sci.* **1996**, *184*, 680.

(7) Machesky, M. L.; Wesolowski, D. J.; Palmer, D. A.; Ridley, M. K. *J. Colloid Interface Sci.* **2001**, *239*, 314.

(8) Jones, P.; Hockey, J. A. *Trans. Faraday Soc.* **1971**, *67*, 2679.

(9) Pauling, L. *J. Am. Chem. Soc.* **1929**, *51*, 1010.

(10) Stern, O. *Z. Elektrochem.* **1924**, *30*, 508.

(11) Westall, J. C.; Hohl, H. *Adv. Colloid Interface Sci.* **1980**, *12*, 265.

(12) Ridley, M. K.; Machesky, M. L.; Wesolowski, D. J.; Palmer, D. A. *Geochim. Cosmochim. Acta* **2004**, *68*, 239.

(13) Ridley, M. K.; Machesky, M. L.; Palmer, D. A.; Wesolowski, D. J. *Colloids Surf. A: Physicochem. Eng. Aspects* **2002**, *204*, 295.

(14) Bedzyk, M. J.; Bommarito, G. M.; Caffrey, M.; Penner, T. L. *Science* **1990**, *248*, 52.

(15) Fenter, P.; Cheng, L.; Rihs, S.; Machesky, M.; Bedzyk, M. J.; Sturchio, N. C. *J. Colloid Interface Sci.* **2000**, *225*, 154.

(16) Bandura, A. V.; Kubicki, J. D. *J Phys. Chem. B* **2003**, *107*, 11072.

(17) Bandura, A. V.; Sykes, D. G., Kubicki, J. D. Adsorption of water on the TiO2 (rutile) [110] surface: A DFT study. *J. Phys. Chem. B* **2004**, *108*, 7844.

(18) Berendsen, H. J. C.; Grigera, J. R.; Straatsma, T. P. *J. Phys. Chem.* **1987**, *91*, 6269.

(19) Sorensen, J. M.; Hura, G.; Glaeser, R. M.; Head-Gordon, T. *J. Chem. Phys.* **2000**, *113*, 9149.

(20) Palmer, B. J.; Pfund, D. M.; Fulton, J. L. *J. Phys. Chem.* **1996**, *100*, 13393.

(21) Lee, S. H.; Rasaiah, J. C. *J. Phys. Chem.* **1996**, *100*, 1420.

(22) Halley, J. W.; Rustad, J. R.; Rahman, A. *J. Phys. Chem.* **1993**, *98*, 4110.

(23) Corrales, L. R. *J. Chem. Phys.* **1999**, *110*, 9071.

(24) Zhang, Z.; Fenter, P.; Cheng, L.; Sturchio, N. C.; Bedzyk, M. J.; Předota, M.; Bandura, A.; Kubicki, J.; Lvov, S. N.; Cummings, P. T.; Chialvo, A. A.; Ridley, M. K.; Bénézeth, P.; Anovitz, L.; Palmer, D. A.; Machesky, M. L.; Wesolowski, D. J. *Langmuir* **2004**, *20*, 4954.

(25) Lindan, P. J. D.; Harrison, N. M.; Gillan, M. J. *Phys. Rev. Lett.* **1998**, *80*, 762.

(26) Diebold, U. *Surf. Sci. Rep.* **2003**, *48*, 53.

(27) Matsui, M.; Akaogi, M. *Mol. Sim.* **1989**, *6*, 239.

(28) Yeh, I.-C.; Berkowitz, M. L. *J. Chem. Phys.* **1999**, *111*, 3155.

(29) Fedkin, M. V.; Zhou, X. Y.; Kubicki, J. D.; Bandura, A. V.; Lvov, S. N.; Machesky, M. L.; Wesolowski, D. J. *Langmuir* **2003**, *19*, 3797.

(30) Smith, P. E.; van Gunsteren, W. F. *Chem. Phys. Lett.* **1993**, *215*, 315.

(31) Lamanna, R., Delmelle, M.; Cannistraro, S. *Phys. Rev. E* **1994**, *49*, 2841.

(32) Mattke, T.; Kecke, H.-J. *J. Colloid Interface Sci.* **1998**, *208*, 562.

(33) Raviv, U.; Klein, J. *Science* **2002**, *297*, 1540.

(34) Předota, M.; Cummings, P. T.; Zhang, Z.; Fenter, P.; Wesolowski, D. J. *J. Phys. Chem. B* **2004**, *108*, 12061–12072 (following paper in this issue).